applied sciences

MDPI

Article

Pore Structure of Coastal Saline Alkali Soil Under Frost Heave at Different Freezing Temperatures by NMR

Kuiqing Liu and Chuanxiao Liu *

College of Water Conservancy and Civil Engineering, Shandong Agricultural University, Tai'an 271018, China; lkq19991213@163.com
* Correspondence: lchuanx@163.com

Abstract

The degradation of soil physical properties, particularly the poorly developed pore structure, is the primary internal factor limiting the productivity of coastal saline alkali soils in the Yellow River Delta. Winter frost heave modifies soil micropores, permeability, and water-salt transport. Conventional techniques, such as polarizing microscopy, scanning electron microscopy, and mercury intrusion porosimetry, cannot characterize soil pore structure accurately and non-destructively. Nuclear magnetic resonance (NMR) was used to investigate the effects of frost heave on the micropore structure and porosity of soil cores (0–40 cm depth) collected from coastal saline alkali land and prepared in the laboratory. Frost heave restructured pore-size distribution, converting micropores into mesopores and macropores. At −15 °C, macropore proportion, cumulative aeration pore proportion, and total porosity peaked across all soil layers. Below −15 °C, reverse compressive stress from ice crystals compressed macropores, thereby reducing porosity. Overall, frost heave improved the aeration and drainage capacity of the otherwise compact soil, rather than merely increasing its total pore volume. These findings provide a reference for pore regulation and soil amelioration in seasonally frozen coastal saline alkali regions.

Keywords: soil microstructure; temperature; frost heave; coastal saline alkali soils; nuclear magnetic resonance

1. Introduction

Soil salinization constrains sustainable agricultural development worldwide and threatens crop growth. By 2050, salinized land across the globe is projected to exceed 50% of the present cultivated-land area [1]. In China, saline alkali soils cover approximately 36 million hm^2, accounting for 4.9% of exploitable land resources [2]. Among these, coastal saline alkali lands reach 5 million hm^2, representing vital reserve land resources yet posing great challenges for reclamation [3]. The Yellow River Delta holds abundant reserve land resources. Nevertheless, influenced by marine sedimentary conditions and shallow, highly mineralized groundwater, local soils exhibit a poorly developed pore structure and low permeability, which directly restrict soil water-salt transport and constitute a major internal cause of severe regional soil salinization [4]. As a seasonally frozen region, the Yellow River Delta experiences repeated freeze–thaw events in winter and spring. The phase transition between pore water and ice crystals modifies soil pore structure, and pore-structure evolution varies with freezing temperature, further altering soil permeability and water-salt transport. Therefore, exploring the pore-structure evolution of saline alkali soils driven by freezing temperature is scientifically significant for revealing the intrinsic mechanisms of frost-heave-regulated water-salt transport in coastal saline alkali soils.

Check for updates

Received: 11 October 2026
Revised: 13 November 2026
Accepted: 20 November 2026
Published: 24 November 2026

Copyright: © 2026 by the authors. Licensee MDPI, Basel, Switzerland. This article is an open access article distributed under the terms and conditions of the Creative Commons Attribution (CC BY) license.

In recent years, numerous studies have addressed the pore-structure evolution of saline alkali soils subjected to frost heave during freeze–thaw events. Qin et al. performed multi-factor laboratory freeze–thaw cycle experiments and revealed how pore evolution affects soil permeability under different regulation measures [5]. Hou et al. indicated that soil water content and temperature directly modify pore volume, quantity, and spatial distribution in frost-affected saline alkali soils [6]. Liu et al., Shen et al., and Liu et al. demonstrated that the number of freeze–thaw cycles substantially changes soil pore morphology, connectivity, and mechanical properties [7–9]. Wang et al. reported that salt content considerably influences the porosity of saline alkali soils after freezing [10]. Overall, existing studies on the pore characteristics of frost-affected saline alkali soils have mainly focused on external factors, including freeze–thaw cycle frequency, water content, and salt content. Research on pore-structure evolution in coastal saline alkali soils driven by varied freezing temperatures remains scarce. Moreover, conventional soil-microstructure techniques such as scanning electron microscopy (SEM), mercury intrusion porosimetry (MIP), and polarizing microscopy cannot provide accurate, non-destructive measurement across the full pore-size range. Nuclear magnetic resonance (NMR) offers a promising alternative for investigating pore-structure changes in saline alkali soils subjected to frost heave.

The limitations of conventional techniques have been widely documented. SEM provides only two-dimensional images of a prepared surface and is sensitive to sample drying, coating, section orientation, and imaging parameters, which restricts its ability to quantify the full pore network [11]. XRD characterises mineral composition rather than pore geometry, whereas MIP forces mercury into pores under high pressure; this pressure can compress or damage fragile aggregates, and the cylindrical-pore assumption introduces "ink-bottle" and isolated-pore errors. Direct comparisons further show that NMR and MIP do not always agree, particularly for fine and poorly connected pores [12]. In contrast, ^{1}H NMR relaxometry detects the hydrogen protons of pore water without drying, coating, or intrusion, and therefore preserves the original structure. A single measurement yields a continuous T_2 distribution that can be converted into a quantitative, full range pore size distribution [13], and the method has been successfully applied to track trimodal pore evolution and freeze–thaw damage in seasonally frozen soils [14]. Its non-destructive, repeatable, and quantitative nature makes NMR particularly suitable for resolving pore changes under a temperature gradient.

Numerous studies have focused on artificial amelioration approaches for saline alkali soils. Biochar application improves soil aggregation and pore-structure properties and enhances permeability owing to its inherent porous features [15,16]. Desulfurized gypsum amendments modify colloidal properties via ion-exchange reactions and indirectly regulate pore development [17,18]. Returning organic materials such as straw promotes aggregate formation during decomposition and expands effective soil pores [19,20]. Physical tillage practices, including subsoiling and deep-ridge tillage, break compact soil layers through mechanical disturbance, directly enlarging pore space and improving the water-salt transport capacity of saline alkali soils [21,22]. Nevertheless, studies on the pore-structure evolution of saline alkali soils under natural frost heave at different freezing temperatures remain limited.

In this study, soil cores (0–40 cm depth) were collected from Linhe Village, Chenzhuang Town, Lijin County, Dongying City, Shandong Province, and prepared in the laboratory for NMR measurements. We investigated the reshaping effects of frost heave on pore size, pore types, and porosity of coastal saline alkali soils under five freezing temperatures (−5 °C, −10 °C, −15 °C, −20 °C, and −25 °C) and identified the freezing temperature associated with the greatest pore-structure development under frost heave. This study aims to provide basic data and a reference for the structural improvement of coastal saline alkali soils.

The novelty of this study is threefold. First, a continuous gradient of five freezing temperatures isolates the temperature effect on pore evolution, whereas previous studies focused mainly on cycle frequency, water content, and salt content. Second, ^{1}H NMR relaxometry provides non-destructive, quantitative measurements across the full pore-size range, avoiding the two-dimensional, preparation, and high-pressure limitations of SEM and MIP [23]. Third, the results identify a critical freezing temperature around −15 °C for aeration-pore development, consistent with previous NMR and freeze–thaw studies [24,25].

2. Materials and Methods

2.1. Study Area

The study site, Linhe Village, Chenzhuang Town, Lijin County, Dongying City, Shandong Province (37°40′27″ N, 118°34′52″ E), lies within the Yellow River Delta (Figure 1). The area has flat, open terrain and gentle coastlines. Located at mid-latitudes, facing the sea and backed by land, it has a warm-temperate, semi-humid, continental monsoon climate with four distinct seasons: dry and windy springs; hot, rainy, and humid summers; cool autumns with sharply reduced rainfall; and cold, dry winters with scarce precipitation, dominated by north and northwest winds. Annual temperatures vary considerably across the year.



Figure 1. Study-area map and field sampling photograph (Lijin County, Dongying City).

The mean annual temperature ranges from 11.7 to 12.6 °C, with extreme maximum and minimum temperatures of 41.9 and −23.3 °C, respectively. The mean annual sunshine duration is 2590–2830 h, and the frost-free period lasts 211 days. Mean annual precipitation varies from 530 to 630 mm, 70% of which occurs in summer, while the mean evapotranspiration ranges between 750 and 2400 mm. Uneven seasonal precipitation leads to prolonged drought periods and salt accumulation at the soil surface, resulting in severe salt-alkali efflorescence at the sampling site. Furthermore, shallow, marine-derived groundwater with high salt concentrations prevails across the Yellow River Delta and readily triggers secondary soil salinization.

Based on the local thermal regime, five freezing temperatures (−5 °C, −10 °C, −15 °C, −20 °C, −25 °C) were selected as experimental variables to investigate how freezing temperature affects frost-heave-induced pore-structure changes in saline alkali soils.

2.2. Experimental Materials

Undisturbed soil cores were collected from undeveloped land in Linhe Village, Chenzhuang Town, Lijin County, Dongying City, Shandong Province. Sampling was performed to a depth of 40 cm, and three replicate samples were obtained at each 10 cm depth interval

to ensure adequate representativeness (Figure 2). Prior to the laboratory tests, all cores were oven-dried at 105 °C. The water content of each soil layer was calculated from the soil mass measured before and after oven-drying. Because the measured water contents varied little across soil layers, a uniform initial water content of 23% was adopted for all soil layers in this experiment.

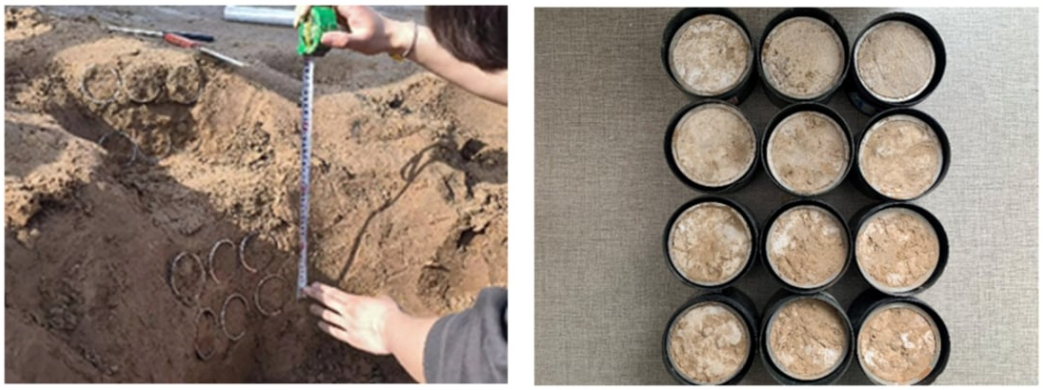

Figure 2. Photographs of field sampling.

Before the freezing tests, the basic physical and chemical properties of the undisturbed soils were determined following standard laboratory procedures. Dry bulk density and gravimetric water content were measured by the oven-drying method; the particle size distribution was analysed by laser diffraction; soil salt content was derived from the electrical conductivity of 1:5 soil–water extracts; pH was measured with a pH meter; and the concentrations of Na^+, K^+, Ca^{2+}, and Mg^{2+} were determined by flame photometry. The initial physicochemical properties of the four soil layers are summarised in Tables 1–3.

Table 1. Physical properties of the tested coastal saline alkali soils at different depths.

Property	10 cm	20 cm	30 cm	40 cm
Dry bulk density ($g \cdot cm^{-3}$)	1.61 ± 0.03	1.54 ± 0.01	1.56 ± 0.01	1.64 ± 0.03
Initial water content (%)	22.81 ± 2.53	21.57 ± 0.96	25.91 ± 0.60	22.47 ± 0.46
Initial NMR porosity (%)	20.23 ± 0.83	17.72 ± 0.80	26.85 ± 0.88	23.15 ± 0.78
Soil texture	Loamy sand	Sandy loam	Silt loam	Silt loam

Values are mean ± standard deviation ($n = 3$).

Table 2. Particle size composition of the tested coastal saline alkali soils at different depths.

Property	10 cm	20 cm	30 cm	40 cm
Clay (%)	2.08	4.07	7.27	4.83
Silt (%)	10.37	25.07	54.70	52.23
Sand (%)	87.55	70.86	38.03	42.94
d10 (μm)	16.94	5.04	2.56	4.21
d60 (μm)	50.79	38.33	19.17	23.29
Cu	3.00	7.61	7.49	5.53
Cc	1.27	2.18	1.39	1.41

Table 3. Chemical properties of the tested coastal saline alkali soils at different depths.

Property	10 cm	20 cm	30 cm	40 cm
Salt content ($g \cdot kg^{-1}$)	6.73 ± 0.31	5.29 ± 0.22	3.19 ± 0.36	2.35 ± 0.42
pH	9.6 ± 0.40	9.3 ± 0.23	9.4 ± 0.12	9.3 ± 0.17
SAR ($(mmol \cdot L^{-1})^{1/2}$)	34.33 ± 0.03	34.46 ± 0.32	33.38 ± 0.74	29.17 ± 1.51
ESP (%)	50.50 ± 0.04	50.70 ± 0.48	49.07 ± 1.11	42.75 ± 2.26
Na^+ ($mg \cdot kg^{-1}$)	16,835 ± 202	16,175 ± 258	15,032 ± 351	12,672 ± 451
K^+ ($mg \cdot kg^{-1}$)	807 ± 15	758 ± 20	708 ± 16	663 ± 25
Ca^{2+} ($mg \cdot kg^{-1}$)	2120 ± 24	1964 ± 96	1802 ± 56	1697 ± 79
Mg^{2+} ($mg \cdot kg^{-1}$)	910 ± 46	820 ± 26	759 ± 36	694 ± 13

Values are mean ± standard deviation ($n = 3$).

These baseline data reveal a compact, strongly alkaline, and sodium-dominated soil. The dry bulk densities (1.54–1.64 g cm^{-3}) exceed the typical range of 1.1–1.4 g cm^{-3} for agricultural soils and indicate a dense structure with poorly developed pores that impedes salt discharge. The gravimetric water contents remain high (21.57–25.91%), consistent with the saline conditions of the site. Salt content and pH decrease slightly with depth, and the 0–20 cm layers are strongly salinised (5.29–6.73 g kg^{-1}) and strongly alkaline (pH 9.3–9.6). The particle size composition changes from coarse, sand-dominated loamy sand at 10 cm to finer silt loam below 20 cm, where the silt fraction rises above 50%. The high Na^+ concentrations and SAR values (29.17–34.46) indicate a sodic environment in which the dispersion of clay particles tends to block the pores and reduce permeability, providing the structural context for the subsequent freezing experiments.

2.3. Sample Preparation

To meet the requirements of the NMR measurements, the oven-dried soil cores were cut with a saw and polished with sandpaper to produce cylindrical specimens 30 mm in height and 15 mm in inner diameter. After cutting and polishing, the specimens from each sampling depth were weighed and their masses recorded. Each specimen was then fitted into an acrylic mould (35 mm in height, 15 mm in inner diameter) that was open at the top and sealed at the bottom, and a corresponding amount of deionized water was added according to the mass of each specimen. The moulds were covered with plastic film and kept in darkness until the water had fully infiltrated the specimens, yielding test specimens with a water content of 23%. The prepared specimens were placed in a high-low temperature test chamber and frozen isothermally for 12 h at −5 °C, −10 °C, −15 °C, −20 °C, and −25 °C, respectively. After freezing, the specimens were thawed at room temperature (+20 °C) for 12 h. Thawing was performed to observe the influences of frost-heave-induced stress on soil pores and to facilitate the subsequent saturation procedure for NMR measurements. Control specimens with an initial water content of 23% but no freezing treatment were also prepared. Three replicate specimens were prepared for each freezing temperature and each soil depth, and the NMR values reported in the results are the means of these three replicates. Because the NMR measurements were performed after thawing and re-saturation, the reported structure is the post-cryogenic (post-thaw) structure produced by the complete freeze–thaw cycle, not the structure of the soil in its frozen state. Pore sizes cannot be measured directly in the frozen state with the present method. In frozen water, the mobility of ^1H protons is strongly reduced and the transverse relaxation time becomes extremely short (on the order of microseconds), so the signal decays within the first few echoes of the CPMG sequence and cannot be captured with the available echo spacing. In addition, the relaxation mechanism of ice differs from that of liquid water, and the surface-relaxivity relationship cannot be used to convert the T_2 of ice into pore

dimensions. Thawing followed by re-saturation therefore uses liquid water as a probe to quantify the pore network reshaped by frost-heave stress.

The plastic film was removed and the specimen masses were measured. Each specimen was saturated by progressively adding deionized water in the open-top, bottom-sealed acrylic mould. Water was applied with a dropper to maintain a layer approximately 5.0 mm above the specimen surface, which allowed water to enter the pore network freely under capillary action. The specimen together with its mould was weighed at regular intervals; the directly measured quantity was the specimen mass, from which the water content was derived. As water was drawn into the pores, the specimen mass increased. When two successive mass measurements taken 2 h apart showed no further increase, the specimen was judged to be saturated, because no additional water was being drawn into the pore network. The saturated specimens were wrapped with plastic film to prevent water loss during NMR measurement (Figure 3). The control specimens followed exactly the same cutting, re-wetting, and saturation steps, the only difference being that they were not subjected to the freezing treatment.



Figure 3. Saturation treatment of soil samples.

2.4. Measurement Methods

NMR can rapidly capture the water content of geomedia via nuclear magnetic signals and accurately characterize water-distribution patterns. It provides a fast and non-destructive approach for characterizing water distribution and micropore structure in geomedia. Compared with other measurement techniques, NMR offers the advantages of convenient and rapid testing, non-destructive specimen analysis, and high-resolution, high-precision outputs [26].

In this study, a 2 MHz LIME-MRI-D2 magnetic resonance analyzer (Beijing Qingmeng Aike Technology Co., Ltd., Beijing, China) was used to investigate pore-structure variations in saline alkali soils (Figure 4). This low-field instrument operates at a ^{1}H (proton) resonance frequency of 2 MHz; all measurements therefore detected the hydrogen-1 nucleus (protons, ^{1}H) of the water molecules retained in the soil pores. The Corespec software was employed for signal acquisition, and the POLIMAR advanced NMR imaging and spectrum-processing software was adopted for data analysis. A 1-inch radio-frequency probe was selected

according to the specimen dimensions, and the Carr-Purcell-Meiboom-Gill (CPMG) pulse sequence was applied for measurements.

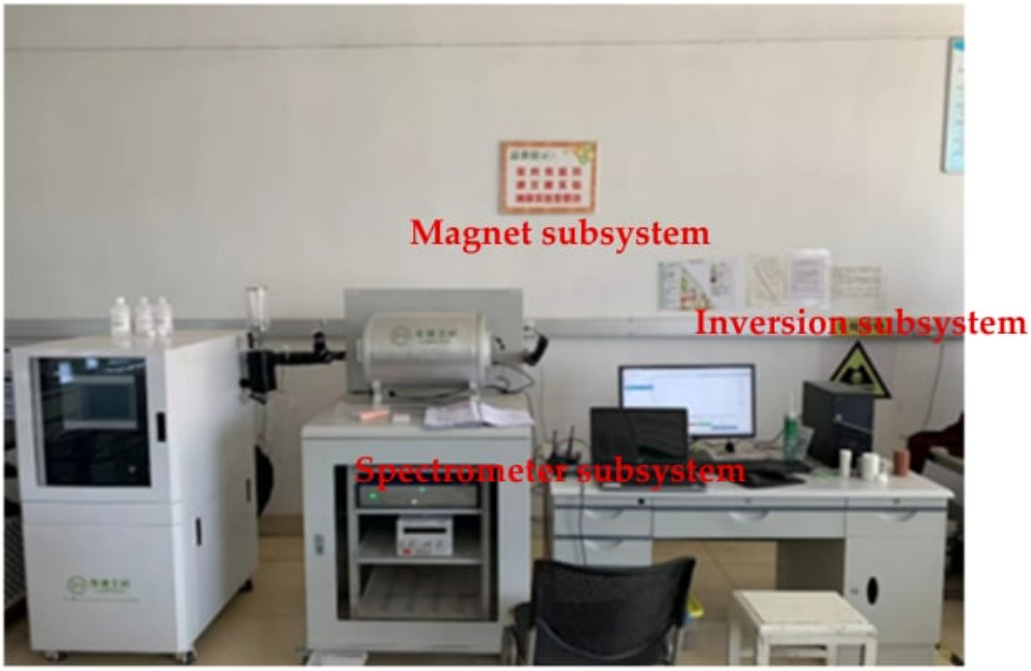

Figure 4. Nuclear magnetic resonance instrument.

The CPMG sequence yields curves describing the variation in nuclear magnetic signals over time. Fourier transformation of these curves generates T_2 (transverse relaxation time) distribution curves. The peak area beneath a curve (i.e., the nuclear magnetic signal, dimensionless) represents the water content corresponding to a given T_2 range. For water-saturated specimens with pores fully filled with water, the T_2 distribution curve characterizes the pore-size-distribution features of the soil. The relationship between T_2 relaxation time and pore size is expressed as Equation (1) [27]:

$$\frac{1}{T_2} = \rho_2 \left(\frac{S}{V} \right)_{\text{pore}} \tag{1}$$

where T_2 represents transverse relaxation time (s); ρ_2 denotes surface relaxivity ($\mu m \cdot s^{-1}$); S denotes pore-surface area (μm^2); V denotes pore volume (μm^3).

In Equation (1), ρ_2 is a constant related to the intrinsic properties of porous media and associated with solid–liquid interfacial interactions [28]. Referring to previous soil-pore studies [29], ρ_2 was assigned a value of 10 $\mu m \cdot s^{-1}$. The S/V ratio depends on pore size. Pore geometry in soils can be approximated as spherical, yielding $S/V = 3/r$. Accordingly, Equation (1) can be rewritten as Equation (2):

$$\frac{1}{T_2} = \frac{30}{r} \tag{2}$$

where r represents pore radius (μm).

The value of ρ_2 was adopted from previous studies on soils. It should be noted that ρ_2 was not independently calibrated for the soils in this study and that the spherical pore geometry is an idealisation, so the absolute pore radii carry uncertainty. However, because the same ρ_2 and geometry were applied to every specimen, the relative comparisons across freezing temperatures including the shift in the T_2 peaks, the proportions of pore types, and the −15 °C threshold do not depend on the exact value of ρ_2, and the principal conclusions remain robust.

Concerning the effect of dissolved salts and paramagnetic impurities, the relaxation of pore water comprises bulk, surface, and diffusion contributions. Dissolved ions, especially paramagnetic species such as Fe and Mn, enhance bulk relaxation and shorten the measured T_2. In this study, the specimens were re-saturated with deionized water and all specimens followed the same preparation and measurement procedure, so these contributions were kept consistent across specimens. In fine pores, surface relaxation is the dominant term. Although dissolved salts and paramagnetic impurities affect the absolute T_2 and therefore the absolute pore radii, they do not alter the relative comparisons because the same constant ρ_2 was applied throughout; this is consistent with the uncertainty in the absolute pore radii stated above.

3. Results

3.1. Pore Size Distribution of Saline Alkali Soils Under Different Freezing Temperatures

According to Equation (2), T_2 is directly proportional to pore radius under saturated conditions. Thus, the pore-size distribution of each specimen group can be derived from the transverse relaxation time data obtained via NMR. Figure 5 shows the pore-size-distribution curves for specimens from different soil layers exposed to various freezing temperatures.

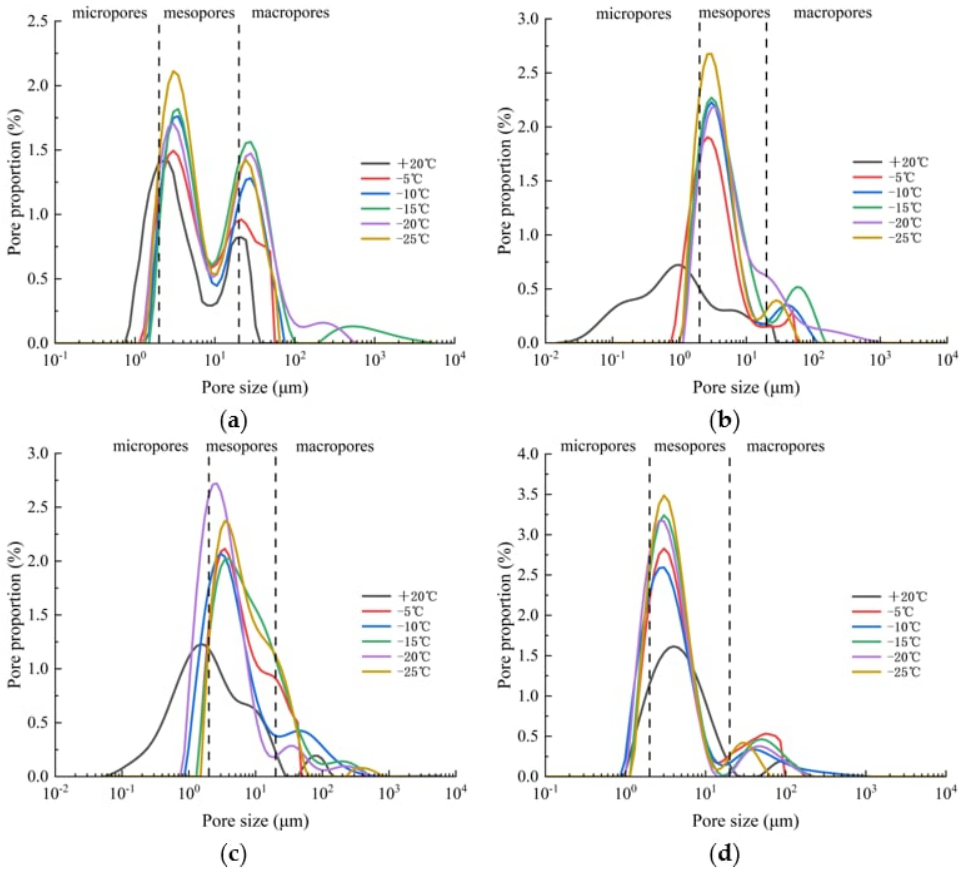

Figure 5. Pore size distribution curves of saline alkali soils under different freezing temperatures: (**a**) 10 cm soil layer; (**b**) 20 cm soil layer; (**c**) 30 cm soil layer; (**d**) 40 cm soil layer.

To further analyze the pore-size variations in specimens from different soil layers under various freezing temperatures, pores were classified into macropores ($d \geq 20$ μm), mesopores (2 μm $< d <$ 20 μm), and micropores ($d \leq 2$ μm), following the criteria of Shear et al. [30] and taking into account the pore-size features of saline alkali soils in the Yellow River Delta. As shown in Figure 5, under the non-freezing control condition (+20 °C), the

pore-size-distribution curves of the 0–40 cm saline alkali soils predominantly exhibited a bimodal pattern with primary and secondary peaks, whereas the 20 cm layer showed a unimodal distribution, indicating a relatively narrow intrinsic pore-size distribution in each layer. The 10 cm and 40 cm layers were dominated by mesopores, while the 20 cm and 30 cm layers consisted mainly of micropores. Pore sizes in the 10 cm layer were concentrated within 0.86–32.32 μm with good continuity. For the 30 cm and 40 cm layers, the primary and secondary peaks were clearly separated, indicating poor pore continuity. Specifically, in the 30 cm layer the primary peak ranged from 0.05 to 28.11 μm and the secondary peak from 49.12 to 130.46 μm; in the 40 cm layer the primary peak covered 0.99–24.45 μm and the secondary peak 49.12–172.46 μm. The 20 cm layer displayed a concentrated unimodal feature, with pore sizes in the range of 0.02–24.45 μm. Overall, the tested coastal saline alkali soils from the Yellow River Delta were dominated by small pores, with poorly developed macropores and a dense intrinsic pore structure, which constitutes the internal micro-scale reason for the low soil permeability in this region. The intrinsic differences in pore morphology are closely related to the particle size composition (Table 2). The 10 cm layer, containing 87.55% sand with a low uniformity coefficient ($C_u = 3.00$), consists of relatively uniform particles and therefore shows a continuous pore-size range. The 20 cm layer has a higher silt fraction and a well-graded distribution ($C_u = 7.61$), so fine particles fill the intergranular voids and produce a concentrated, unimodal pore distribution dominated by micropores. In the 30 cm and 40 cm layers, the silt fraction exceeds 52% and coarse and fine particles are mixed, which separates the two peaks and weakens pore continuity. The high dry bulk densities (1.54–1.64 g cm^{-3}, above the 1.1–1.4 g cm^{-3} range of agricultural soils), together with the high Na^+ concentration and SAR (Table 3), promote clay dispersion and pore clogging, accounting for the dense, fine-pore-dominated fabric and the low permeability of these soils.

After the freezing treatments, the pore-size-distribution curves of all soil layers shifted toward larger pore sizes: the intensity of the peaks corresponding to large pores increased, and new peaks appeared in some soil layers. These observations indicate that the water-ice phase transition induced by frost heave can restructure soil pore structure, with some original micropores expanding and new pores being generated.

Based on the classification introduced above, the proportions of macropores, mesopores, and micropores were calculated for each soil layer under each freezing temperature, as shown in Figure 6.

Figure 6 shows the proportions of macropores, mesopores, and micropores in each soil layer under the different freezing-temperature treatments. In the control group, the 10 cm and 40 cm soil layers were dominated by mesopores, whereas the 20 cm and 30 cm soil layers were dominated by micropores. Compared with the unfrozen controls, the 10–30 cm soil layers generally showed a decrease in the micropore proportion and an increase in the meso- and macropore proportions after freezing, indicating that pore evolution within this depth interval was mainly characterized by the conversion of micropores into larger pores. Pore evolution in the deep 40 cm soil layer was more complex: the proportions of all pore categories increased to varying degrees, suggesting that, in addition to the conversion of micropores into meso- and macropores, new micropores were simultaneously generated, and that the generation rate of new micropores may have exceeded the conversion rate of micropores towards larger pore sizes.

Freezing temperature directly influenced pore reshaping. Under the −5 °C treatment, the micropore proportion decreased distinctly while the meso- and macropore proportions increased in the 10, 20, and 30 cm soil layers. All pore-type proportions rose simultaneously in the 40 cm soil layer, with greater increments for meso- and macropores than for microp-

ores, indicating that frost heave at −5 °C promoted micropore expansion in the 10–30 cm layers while generating new pores alongside pore expansion in the 40 cm layer.

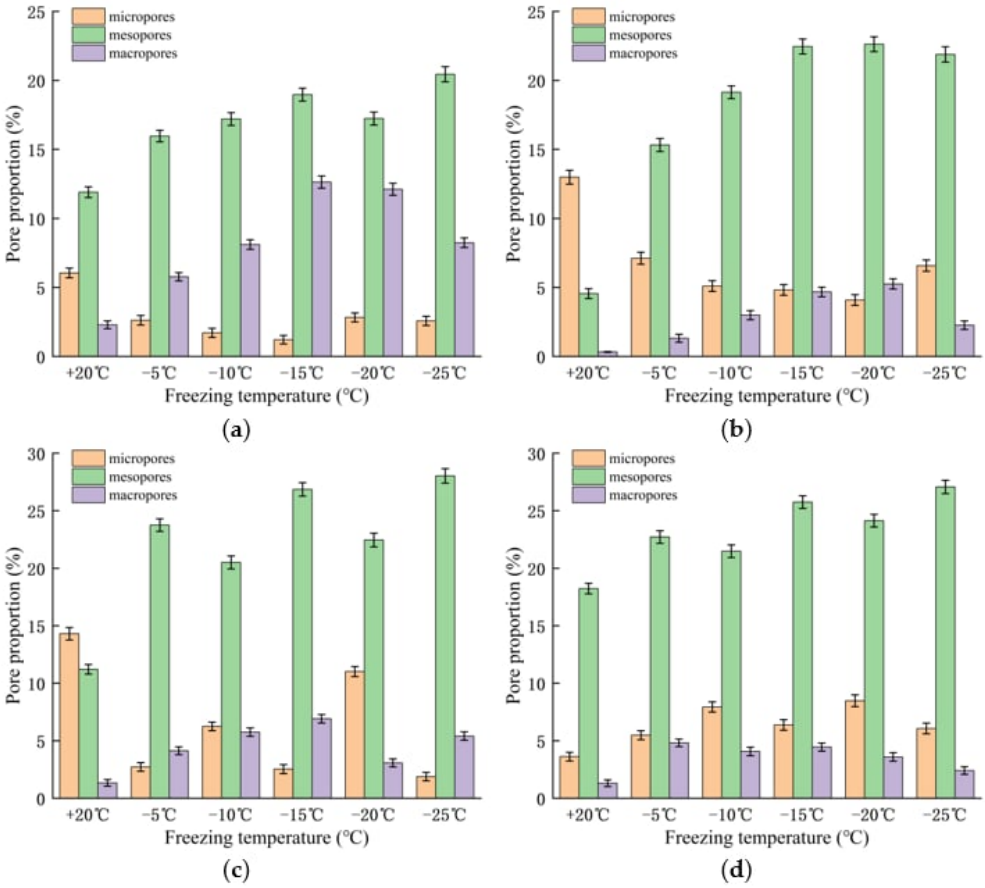

Figure 6. The proportion of pore size in saline alkali soil at different freezing temperatures: (**a**) 10 cm soil layer; (**b**) 20 cm soil layer; (**c**) 30 cm soil layer; (**d**) 40 cm soil layer. Error bars represent standard deviations of three repls.

When the freezing temperature decreased to −10 °C, micropore proportions kept declining and meso- and macropore proportions kept rising in the 10 cm and 20 cm soil layers, whereas micropore proportions rebounded in the 30 cm and 40 cm soil layers. Some mesopores were further converted into macropores in the 30 cm soil layer, and newly formed micropores exerted a certain squeezing effect on pre-existing meso- and macropores in the 40 cm soil layer.

At −15 °C, all soil layers showed reduced micropore proportions and markedly elevated meso- and macropore proportions. The macropore proportions of the 10 cm and 30 cm soil layers reached their maxima in this experimental set; the mesopore proportion peaked in the 20 cm soil layer and approached its maximum in the 40 cm soil layer. Within the tested temperature gradient, the conversion of micropores into meso- and macropores was most prominent at −15 °C.

Upon further cooling to −20 °C, micropore proportions rebounded and meso- and macropore proportions dropped in the 10, 30, and 40 cm soil layers. Only in the 20 cm soil layer did micropores continue to convert into meso- and macropores, yet the increment slowed markedly and the pore-improving effect of low temperature decayed.

When the temperature was further lowered to −25 °C, pore-evolution patterns varied across soil layers. In the 10 cm soil layer, micropores were mainly transformed into mesopores, and macropore proportions declined because of squeezing. Newly generated

micropores inhibited macropore development in the 20 cm soil layer. In the 30 cm soil layer, micropores were mostly converted into mesopores, and increased mesopores and compressed macropores were similarly observed in the 40 cm soil layer. Overall, cooling below −15 °C was detrimental to the continued development of soil macropores.

3.2. Pore Types of Saline Alkali Soils Under Different Freezing Temperatures

Based on pore-structure classification criteria, soil pores can be divided into three categories. Pores with a diameter smaller than 0.002 mm are defined as inactive pores, which represent the finest soil pores and are inaccessible to microorganisms and plant root hairs. Pores ranging from 0.002 to 0.02 mm are capillary pores; they exhibit prominent capillary effects and serve as the major sites for soil-water storage and intensive water movement. Pores larger than 0.02 mm are aeration pores. Water held in aeration pores is readily drained under gravity, favouring soil-water infiltration [31]. The pores of saline alkali soils under different freezing-temperature treatments were classified following these criteria, and the results are summarised in Table 4. These three functional classes correspond to the size-based classes used in Section 3.1: inactive pores correspond to micropores ($d \leq 2$ μm), capillary pores to mesopores (2–20 μm), and aeration pores to macropores ($d \geq 20$ μm). The two systems therefore share the same diameter thresholds and differ only in terminology.

Table 4. Proportions of pore types in saline alkali soils under different freezing temperatures.

Soil Layer	Temperature (°C)	Inactive Pores (%)	Capillary Pores (%)	Aeration Pores (%)
10 cm	+20 °C	7.46 ± 0.35	10.48 ± 0.39	2.29 ± 0.28
	−5 °C	3.96 ± 0.35	14.62 ± 0.42	5.06 ± 0.30
	−10 °C	3.09 ± 0.33	16.98 ± 0.46	6.95 ± 0.35
	−15 °C	2.54 ± 0.31	17.64 ± 0.47	12.63 ± 0.44
	−20 °C	2.83 ± 0.33	17.23 ± 0.47	12.11 ± 0.44
	−25 °C	2.57 ± 0.33	23.02 ± 0.55	5.66 ± 0.35
20 cm	+20 °C	13.43 ± 0.50	4.29 ± 0.36	0.00 ± 0.03
	−5 °C	8.97 ± 0.44	13.46 ± 0.47	1.32 ± 0.29
	−10 °C	7.12 ± 0.39	17.31 ± 0.47	2.92 ± 0.33
	−15 °C	6.90 ± 0.39	20.57 ± 0.54	4.47 ± 0.35
	−20 °C	5.98 ± 0.39	20.73 ± 0.54	5.25 ± 0.37
	−25 °C	6.57 ± 0.41	21.88 ± 0.56	2.26 ± 0.31
30 cm	+20 °C	15.43 ± 0.54	10.27 ± 0.42	1.15 ± 0.29
	−5 °C	4.43 ± 0.37	22.94 ± 0.55	3.26 ± 0.34
	−10 °C	5.25 ± 0.37	21.88 ± 0.56	5.43 ± 0.37
	−15 °C	5.95 ± 0.39	24.48 ± 0.59	5.87 ± 0.37
	−20 °C	8.41 ± 0.44	25.06 ± 0.60	3.07 ± 0.35
	−25 °C	3.60 ± 0.37	26.31 ± 0.63	5.41 ± 0.37
40 cm	+20 °C	4.92 ± 0.38	16.93 ± 0.46	1.30 ± 0.29
	−5 °C	5.48 ± 0.39	23.00 ± 0.55	2.92 ± 0.33
	−10 °C	7.94 ± 0.44	21.68 ± 0.55	3.88 ± 0.37
	−15 °C	9.27 ± 0.46	22.86 ± 0.55	4.45 ± 0.35
	−20 °C	11.51 ± 0.51	21.16 ± 0.55	3.54 ± 0.37
	−25 °C	9.15 ± 0.46	23.99 ± 0.58	2.41 ± 0.33

Values are mean ± standard deviation ($n = 3$).

The proportion of aeration pores can directly reflect the water-permeable and air-conducting capacity of soil. As shown in Table 4, differences existed in the proportions of inactive, capillary, and aeration pores across soil layers under the different freezing-temperature treatments. At −15 °C, the aeration-pore proportions of the 10, 30, and 40 cm

soil layers reached their maxima within this experiment, amounting to 12.63%, 5.87%, and 4.45%, respectively. For the 20 cm soil layer, the peak aeration-pore proportion of 5.25% occurred at −20 °C. These results indicate that frost heave can effectively increase the proportion of aeration pores in soil and that most soil layers exhibited the most highly developed aeration pores under the −15 °C treatment.

To characterize the overall variation in pore-type proportions over the entire 0–40 cm soil profile in response to freezing temperature, the cumulative proportions of each pore type across the individual soil layers were calculated for each freezing-temperature treatment, and the results are presented in Figure 7.

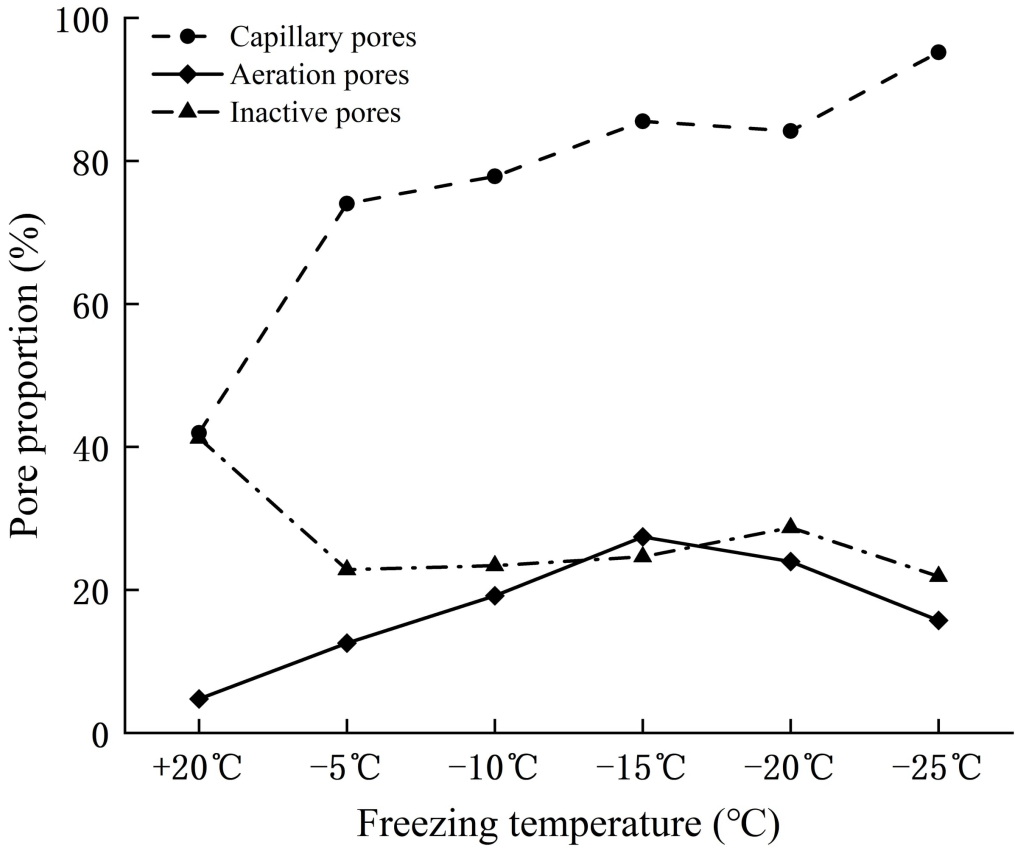

Figure 7. Cumulative proportions of pore types in saline alkali soils under different freezing temperatures.

As shown in Figure 7, the total proportion of aeration pores exhibited an upward-then-downward trend with decreasing freezing temperature. It peaked at 27.42% at −15 °C, while the proportion of inactive pores increased only slightly. This indicates that the soil tended to generate aeration pores preferentially under this temperature condition, without a synchronous substantial increase in fine inactive pores. When the temperature deviated from −15 °C toward either warmer or colder values, the overall proportion of aeration pores decreased.

3.3. Porosity of Saline Alkali Soils Under Different Freezing Temperatures

Frost heave induced by temperature variation can substantially alter soil pore structure. As pore water freezes into ice crystals, its volume increases, and additional pores form after thawing; frost heave can therefore increase soil porosity. As measured by NMR, the initial porosities of the soil layers were 20.23%, 17.72%, 26.85%, and 23.15%, respectively. The variations in porosity with decreasing freezing temperature are shown in Figure 8.

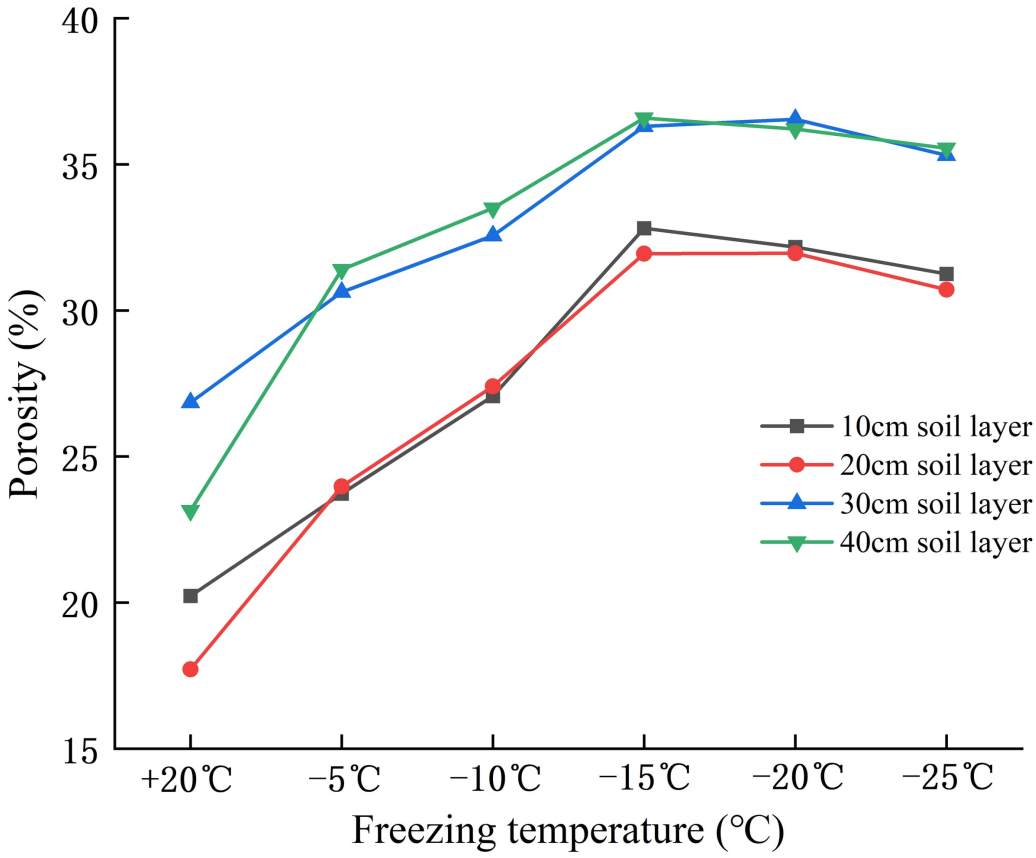

Figure 8. Porosity of saline alkali soils under different freezing temperatures.

As shown in Figure 8, the porosity of each soil layer generally increased and then decreased as freezing temperature declined. Within the range from 0 to −15 °C, porosity rose with decreasing temperature in all soil layers, indicating that frost heave elevated the overall pore level of the soil. When the freezing temperature dropped from −15 to −25 °C, the porosity of each soil layer gradually decreased. Within the temperature gradient adopted in this experiment, the porosity of all soil layers reached its maximum under the −15 °C treatment.

At a soil water content of 23%, most pore water in the soil underwent a phase transition into ice when the freezing temperature was below −15 °C. Combined with the pore-size distribution and pore-type results above, the compressive stress generated by ice crystals at lower temperatures no longer primarily expanded pores. Instead, the reaction force between ice crystals and the soil matrix began to compress internal pore channels, squeezing part of the large pore space and ultimately reducing soil porosity. In addition, the dissolved salts modify the freezing process. Salts lower the freezing point of the pore solution and increase the amount of unfrozen water, and the salt content varies markedly among layers (6.73 g kg^{-1} at 10 cm versus 2.35 g kg^{-1} at 40 cm; Table 3). These differences in pore-solution concentration produce layer-specific freezing points and unfrozen-water contents, which contribute to the distinct frost-heave responses and provide the background conditions for the observed threshold. Because the unfrozen-water content was not measured directly, the interpretation that most free water had frozen below −15 °C and that reverse compression then dominated is an inference based on the observed porosity and pore-type changes rather than a direct measurement.

4. Discussion

Using NMR measurements, this study revealed the evolution patterns of pore structure in 0–40 cm coastal saline alkali soils from the Yellow River Delta subjected to frost heave during freeze–thaw treatments at different freezing temperatures. The intrinsic physical origin of soil-pore modification lies in the phase-transition effect of pore water and ice crystals during frost heave. During the freezing stage, pore water transforms into ice crystals, which expand in volume and exert compressive action on the surrounding soil skeleton. This drives the expansion and connection of original fine pores and even the generation of entirely new pores, ultimately modifying the original pore-size-distribution pattern of the soil. These findings are consistent with recent conclusions on the micropore-structure evolution of saline alkali soils under frost heave in seasonally frozen regions [32,33].

The results of this study indicated that the reshaping of pore structure in coastal saline alkali soils by freezing temperature exhibited a threshold effect. Within the temperature range from 0 to −15 °C, the expansive force generated by growing ice crystals is increasingly exerted on the soil skeleton. Micropores inside the soil continuously transform into mesopores and macropores, and the proportions of aeration pores and total porosity increase simultaneously. When the freezing temperature drops below −15 °C, the reshaping effect on pore structure reverses, accompanied by reductions in macropore proportion and total porosity. Under the laboratory condition of a soil water content of 23%, −15 °C acts as the critical transition temperature for the development of aeration pores in the tested coastal saline alkali soils. This threshold phenomenon arises from the following mechanism: at temperatures above −15 °C, abundant free pore water remains available for phase transition, and ice crystal expansion mainly contributes to the enlargement of pore space. When the temperature decreases further below −15 °C, most free pore water completes the freezing phase change, and no additional free water is available to drive pore expansion. The reverse compressive stress between the ice crystals and the soil skeleton then becomes dominant, compressing the pre-formed large pore channels inside the soil. Some soil aggregates break under stress and produce new tiny pores, which ultimately leads to a decline in macropore proportion and a rebound in micropore proportion [34]. Meanwhile, the pore response to freezing temperature shows remarkable stratification across soil layers: the conversion from micropores to mesopores and macropores dominates in the 10–30 cm soil layers, whereas the deep soil at 40 cm not only experiences micropore expansion but also generates secondary tiny pores. Differences in particle composition and initial pore structure between deep and shallow soils, as well as variations in soil specific surface area and adsorbed bound water content, result in distinct pore-evolution behaviours under frost heave relative to the upper soil layers. This stratification can be traced to the baseline properties in Tables 1–3: the upper 10–30 cm layers are coarser and sand-dominated with lower uniformity coefficients, whereas the 40 cm layer contains more silt (52.23%) and has a larger specific surface area and more adsorbed bound water. The high Na^+ content and SAR (29.17–34.46) further drive clay dispersion, which differs among layers and modifies how the pores respond to ice-crystal growth.

Numerous previous studies have investigated the microscale characteristics of saline alkali soils affected by frost heave during freeze–thaw events. Most of these studies focused on the effects of freeze–thaw cycles, salt content, water content, and other factors on soil pores [35,36], and confirmed that frost heave can alter soil pore morphology, pore connectivity, and mechanical properties. The ice-water phase transition induced by frost heave acts as the core driving force for pore evolution, which is consistent with the conclusion of this study that frost heave can reshape the pore structure of coastal saline alkali soils [37]. Nevertheless, few existing studies have adopted continuous gradients of freezing temperature, and quantitative analysis of pore structure in coastal saline alkali soils remains

insufficient. Most micro-characterization techniques have inherent limitations. Scanning electron microscopy and polarizing microscopy can only obtain two-dimensional sectional morphology of soil, and the statistical results are affected by slice positions, making quantitative analysis across the full pore-size range difficult [38]. The high-pressure intrusion during mercury intrusion porosimetry causes irreversible damage to the fragile aggregate structure of undisturbed soils after frost heave [39]. In this study, NMR was applied to avoid the drawbacks of the conventional observation methods described above, enabling non-destructive quantitative measurement of full-range pore sizes in the tested soils under frost heave. Variations in pore-size distribution, pore-type composition, and porosity at different freezing temperatures were obtained, providing new experimental references for understanding the microscale frost-heave processes of saline alkali soils under seasonally frozen conditions in the Yellow River Delta.

Although complementary SEM, XRD, and MIP measurements were not performed in this study, the adopted ^{1}H NMR approach alone provides non-destructive, full range, and quantitative pore information that is sufficient to address the stated research objectives [40]. A systematic multi technique comparison combining NMR with SEM, XRD, and MIP is therefore identified as a priority for subsequent research. Meanwhile, the multi gradient freezing temperatures designed in this laboratory test were used to simulate field low temperature conditions in winter in the Yellow River Delta. The threshold feature of pore structure evolution obtained here can explain the soil pore structure changes induced by different winter low temperatures in seasonally frozen regions. It also provides a microscale theoretical basis for understanding the variations in field soil permeability and soil water-salt transport during winter and spring. From a practical standpoint, the −15 °C result indicates that moderate freezing promotes the development of aeration pores, which favours drainage and salt leaching in saline alkali soils; this provides a reference for scheduling earthwork and soil improvement operations in seasonally frozen coastal regions.

This study has several limitations. First, the experiment was designed to isolate the effect of freezing temperature. Although the natural salt content differed among soil layers, it was not independently manipulated as a controlled factor to separate its individual effect; all specimens were also adjusted to a single initial water content (23%) and subjected to a single freeze–thaw cycle. Consequently, the conclusions are specific to this water content and cycle condition and should not be generalised directly to other water contents, cycle numbers, or the spatially and temporally variable water contents encountered in the field. Second, the cores were oven-dried, re-wetted, and re-saturated before testing, and the small laboratory specimens are subject to scale effects; the measured pore structures therefore characterise laboratory-prepared, post-thaw, water-saturated specimens rather than the undisturbed field structure, and the effects of the drying–rewetting procedure cannot be fully separated from those of frost heave [41]. The coupled interaction between salt crystallization and frost heave was also not examined. Third, the microstructure was characterized solely by NMR, and complementary SEM, XRD, and MIP analyses were not conducted. Future work should therefore add multiple water-content levels and repeated freeze–thaw cycles, refine the temperature gradient and conduct two-factor coupling experiments, combine NMR with SEM, XRD, and MIP for multi-technique cross-validation, sample additional sites, and carry out in situ field experiments to verify and extend these findings under natural conditions.

Moreover, a fraction of the pore water remains as bound, unfrozen water, particularly the thin films adsorbed on particle surfaces and the water retained in the smallest pores, even at temperatures below −15 °C [42]. Because the unfrozen-water fraction was not quantified in this study, the statement that most pore water transformed into ice should be read as a qualitative interpretation rather than a quantitative claim, and no frozen-water fraction is reported. Quantitative determination of the unfrozen-water content would

require dedicated low-temperature NMR or calorimetric measurements and is left for future work.

5. Conclusions

This study took the 0–40 cm soil cores collected from Linhe Village, Chenzhuang Town, Lijin County, Dongying City, Shandong Province as research objects. Laboratory freezing simulation tests were conducted at an initial water content of 23%, and NMR was used to investigate the effects of frost heave on the pore structure of the coastal saline alkali soils under a gradient of freezing temperatures. The results showed that, under the present experimental conditions, the native pores of the tested coastal saline alkali soils from the Yellow River Delta were poorly developed and dominated by fine pores, leading to a dense soil fabric. Frost heave markedly altered soil porosity. As the freezing temperature decreased, soil porosity generally increased first and then decreased, with −15 °C being the temperature of maximum porosity under the experimental conditions. The conversion of micropores into mesopores and macropores was most prominent at −15 °C. Further cooling below −15 °C was unfavourable for the continuous development of soil macropores, because the reverse squeezing effect of ice crystals compressed part of the macropores. The proportion of aeration pores exhibited a distinct response to freezing temperature, and the total proportion of aeration pores across the soil profile reached 27.42% under the −15 °C treatment.

Author Contributions: Conceptualization, K.L. and C.L.; methodology, K.L.; software, K.L.; validation, K.L. and C.L.; formal analysis, K.L.; investigation, K.L.; resources, C.L.; data curation, K.L.; writing—original draft preparation, K.L.; writing—review and editing, C.L.; visualization, K.L.; supervision, C.L.; project administration, C.L.; funding acquisition, C.L. All authors have read and agreed to the published version of the manuscript.

Funding: This research was funded by the Natural Science Foundation of Shandong Province, grant number ZR2025MS588. The APC was funded by Shandong Agricultural University.

Institutional Review Board Statement: Not applicable.

Informed Consent Statement: Not applicable.

Data Availability Statement: The data presented in this study are available on request from the corresponding author. The data are not publicly available because they were generated from laboratory soil column experiments conducted for this research project.

Acknowledgments: The authors have reviewed and edited the output and take full responsibility for the content of this publication.

Conflicts of Interest: The authors declare no conflicts of interest.

References

1. Hassani, A.; Azapagic, A.; Shokri, N. Global predictions of primary soil salinization under changing climate in the 21st century. *Nat. Commun.* **2021**, *12*, 6663. [CrossRef]
2. Ivushkin, K.; Bartholomeus, H.; Bregt, A.K.; Pulatov, A.; Kempen, B.; De Sousa, L. Global mapping of soil salinity change. *Remote Sens. Environ.* **2019**, *231*, 111260. [CrossRef]
3. Liu, B.; Han, Q.; Wang, S.; Chen, P. Irrigation Regimes Shape Vertical Salt Distribution in Coastal Saline–Alkali Farmlands: A PLS-SEM Analysis of Direct Ion Input and Physicochemical Pathways. *Agronomy* **2026**, *16*, 1661. [CrossRef]
4. Liu, C.; Li, K.; Ma, D. Construction and Engineering Application of Salt-Discharging Model for Local Saline-Alkali Soil with Compact Structure in the Yellow River Delta. *Appl. Environ. Soil Sci.* **2020**, *2020*, 906747. [CrossRef]
5. Qin, Y.; Bai, Y.; Chen, G.; Liang, Y.; Li, X.Y.; Wen, B.; Lu, X.; Li, X.J. The effects of soil freeze–thaw processes on water and salt migrations in the western Songnen Plain, China. *Sci. Rep.* **2021**, *11*, 3888. [CrossRef]
6. Hou, X.; Gao, Y.; Liu, X.; Xu, T.; Xu, J.; Zhao, Y.; Liu, Y. Experimental study on the pore structure and permeability characteristics of clay soil under freezing–thawing cycles. *Sci. Rep.* **2025**, *15*, 31216. [CrossRef]

7. Liu, Y.; Wang, Q.; Liu, S.; ShangGuan, Y.; Fu, H.; Ma, B.; Chen, H.; Yuan, X. Experimental investigation of the geotechnical properties and microstructure of lime-stabilized saline soils under freeze-thaw cycling. *Cold Reg. Sci. Technol.* **2019**, *161*, 32–42. [CrossRef]
8. Shen, J.; Wang, Q.; Chen, Y.; Han, Y.; Zhang, X.; Liu, Y. Evolution process of the microstructure of saline soil with different compaction degrees during freeze-thaw cycles. *Eng. Geol.* **2022**, *304*, 106699. [CrossRef]
9. Liu, X.; Zhang, X.; Shen, J.; Zhang, Y.; Guan, R.; Lv, Q.; Wang, E.; Wang, L.; Jiang, H.; Han, H. Mechanical Properties and Microstructural Evolution of Dispersive Soils Under Freeze–Thaw Cycles. *Water* **2026**, *18*, 2147. [CrossRef]
10. Wang, J.; Wang, Q.; Kong, Y.; Han, Y.; Cheng, S. Analysis of the pore structure characteristics of freeze-thawed saline soil with different salinities based on mercury intrusion porosimetry. *Environ. Earth Sci.* **2020**, *79*, 161. [CrossRef]
11. Tang, C.S.; Cheng, Q.; Gong, X.; Shi, B.; Inyang, H.I. Investigation on microstructure evolution of clayey soils: A review focusing on wetting/drying process. *J. Rock Mech. Geotech. Eng.* **2023**, *15*, 269–284. [CrossRef]
12. Li, C.; Liu, X.; You, F.; Wang, P.; Feng, X.; Hu, Z. Pore Size Distribution Characterization by Joint Interpretation of MICP and NMR: A Case Study of Chang 7 Tight Sandstone in the Ordos Basin. *Processes* **2022**, *10*, 1941. [CrossRef]
13. An, R.; Zhang, X.; Kong, L.; Gong, J.; Lei, X. Artificial Ground Freezing Impact on Shear Strength and Microstructure of Granite Residual Soil Under an Extremely Low Temperature. *Front. Earth Sci.* **2021**, *9*, 772459. [CrossRef]
14. Li, T.; Kong, L.; Wang, J. Trimodal pore-structure evolution and its mechanical effects on expansive soil in seasonally frozen regions based on NMR. *Rock Soil Mech.* **2021**, *42*, 2741–2754. [CrossRef]
15. Wang, P.; Lin, X.; Liu, Q.; Lin, Z.; Yang, Y.; Chen, H.; Fan, S. Interactions between flue gas desulfurization gypsum and biochar on water infiltration characteristics and physicochemical properties of saline-alkaline soil. *Environ. Monit. Assess.* **2023**, *195*, 1273. [CrossRef]
16. Zong, Y.; Wang, Y.; Lv, A.; Xiao, Q.; Malik, Z.; Ma, R.; Ding, X.; Li, Y. Microbial response to physical fertility improvement induced by biochar application to coastal saline-alkali soil, Eastern China. *Arch. Agron. Soil Sci.* **2026**, *72*, 1–16. [CrossRef]
17. Liao, R.; Yu, H.; Yang, P.; Lin, H. Quantitative evaluation of pore characteristics of sodic soils reclaimed by flue gas desulphurization gypsum using X-ray computed tomography. *Land Degrad. Dev.* **2020**, *31*, 545–556. [CrossRef]
18. Wang, Y.; Wang, Z.; Liang, F.; Jing, X.; Feng, W. Application of flue gas desulfurization gypsum improves multiple functions of saline-sodic soils across China. *Chemosphere* **2021**, *277*, 130345. [CrossRef]
19. Xie, W.; Wu, L.; Zhang, Y.; Wu, T.; Li, X.; Ouyang, Z. Effects of straw application on coastal saline topsoil salinity and wheat yield trend. *Soil Tillage Res.* **2017**, *169*, 1–6. [CrossRef]
20. Zhang, H.; Pang, H.; Zhao, Y.; Lu, C.; Liu, N.; Zhang, X.; Li, Y. Water and salt exchange flux and mechanism in a dry saline soil amended with buried straw of varying thicknesses. *Geoderma* **2020**, *365*, 114213. [CrossRef]
21. Chen, J.; Wu, L.; Zhang, X.; Deng, A.; Song, Z.; Zhang, W.; Zheng, C. Effects of Ridge Tillage and Sowing in Furrow on Soil Water and Salt Dynamics and Maize Growth in Coastal Saline-Alkali Land. *Sci. Agric. Sin.* **2025**, *58*, 4259–4271. [CrossRef]
22. Wu, M.; Ma, Y.; Ai, P.; Ma, Z.; Liu, C. Effects of Deep Ploughing Combined with Subsurface Drainage on Soil Water–Salt Dynamics and Physical Properties in Arid Regions. *Sustainability* **2026**, *18*, 862. [CrossRef]
23. Tian, H.; Wei, C.; Wei, H. An NMR-based analysis of soil–water characteristics. *Appl. Magn. Reson.* **2014**, *45*, 49–61. [CrossRef]
24. Liu, Q.; Cai, G.; Han, B. Experimental study on pore structure and freezing characteristics of graded soil based on nuclear magnetic resonance. *Chin. J. Geotech. Eng.* **2022**, *44*, 178–182. [CrossRef]
25. Ma, Q.; Zhang, K.; Jabro, J.D.; Ren, L.; Liu, H. Freeze–thaw cycles effects on soil physical properties under different degraded conditions in Northeast China. *Environ. Earth Sci.* **2019**, *78*, 321. [CrossRef]
26. Yin, M.; Zhang, H.; Zhang, D.; Shi, L.; Li, F.; Xing, B. Exploring the impact of close-cell structures of three-dimensional graphene on BPA adsorption via 1H NMR relaxation and isotope tracing. *Mater. Today Chem.* **2026**, *53*, 103542. [CrossRef]
27. He, Y.; Peng, Q.; Wang, L.; Wang, S.; Nie, L.; Xu, Y.; Lü, Y.; Chen, Y.; Zhang, X. Investigating pore characteristics and permeability of seasonally frozen turfy soil using multiple micro-test methods. *Rock Soil Mech.* **2025**, *46*, 110–122. [CrossRef]
28. Matteson, A.; Tomanic, J.P.; Herron, M.M.; Allen, D.F.; Kenyon, W.E. NMR Relaxation of Clay/Brine Mixtures. *SPE Reserv. Eval. Eng.* **2000**, *3*, 408–413. [CrossRef]
29. Meyer, M.; Buchmann, C.; Schaumann, G.E. Determination of quantitative pore-size distribution of soils with 1H NMR relaxometry. *Eur. J. Soil Sci.* **2018**, *69*, 393–406. [CrossRef]
30. Shear, D.L.; Olsen, H.; Nelson, K. *Effects of Desiccation on the Hydraulic Conductivity Versus Void Ratio Relationship for a Natural Clay*; National Academy Press: Washington, DC, USA, 1993; pp. 1365–1370.
31. An, D.; Peng, X.; Dai, Q. Response of soil pore variation and infiltration to dry-wet changes at rock-soil and non-rock-soil interface in rocky desertification areas. *Trans. Chin. Soc. Agric. Eng. (Trans. CSAE)* **2024**, *40*, 139–149. [CrossRef]
32. Wan, X.; Liu, E.; Qiu, E. Study on ice nucleation temperature and water freezing in saline soils. *Permafr. Periglac.* **2021**, *32*, 119–138. [CrossRef]
33. Zhu, J.; Chen, H.; Wan, X.; Zhao, Y.; Lai, Y. A theoretical model of the hysteresis on the unfrozen water content in soils and its application. *Acta Geotech.* **2026**, *21*, 909–935. [CrossRef]

34. Xia, W.; Niu, C.; Yu, Q.; Wang, Q.; Wang, J.; Sun, X.; Wang, Z.; Shan, X. Experimental investigation of the erodibility of soda saline-alkali soil under freeze-thaw cycle from a microscopic view. *CATENA* **2023**, *232*, 107430. [CrossRef]
35. Han, M.; Peng, W.; Ma, B.; Yu, Q.; Kasama, K.; Furukawa, Z.; Niu, C.; Wang, Q. Micro–composition evolution of the undisturbed saline soil undergoing different freeze–thaw cycles. *Cold Reg. Sci. Technol.* **2023**, *210*, 103825. [CrossRef]
36. Kong, F.; Nie, L.; Xu, Y.; Rui, X.; He, Y.; Zhang, T.; Wang, Y.; Du, C.; Bao, C. Effects of freeze-thaw cycles on the erodibility and microstructure of soda-saline loessal soil in Northeastern China. *CATENA* **2022**, *209*, 105812. [CrossRef]
37. Xu, W.; Li, K.; Chen, L.; Kong, W.; Liu, C. The impacts of freeze–thaw cycles on saturated hydraulic conductivity and microstructure of saline–alkali soils. *Sci. Rep.* **2021**, *11*, 18655. [CrossRef]
38. Cao, Y.; Zhang, K.; Liu, S.; Wang, Y. A review of advancements in the theory and characterization of soil macropore structure. *PeerJ* **2024**, *12*, e18442. [CrossRef]
39. Xue, S.; Zhang, P.; Bao, J.; He, L.; Hu, Y.; Yang, S. Comparison of Mercury Intrusion Porosimetry and multi-scale X-ray CT on characterizing the microstructure of heat-treated cement mortar. *Mater. Charact.* **2020**, *160*, 110085. [CrossRef]
40. Guo, J.C.; Zhou, H.Y.; Zeng, J.; Wang, K.J.; Lai, J.; Liu, Y.X. Advances in low-field nuclear magnetic resonance (NMR) technologies applied for characterization of pore space inside rocks: A critical review. *Pet. Sci.* **2020**, *17*, 1281–1297. [CrossRef]
41. Zhang, X.; Liu, X.; Chen, C.; Xu, Y.; Liu, H. Evolution of disintegration properties of granite residual soil with microstructure alteration due to wetting and drying cycles. *Bull. Eng. Geol. Environ.* **2022**, *81*, 93. [CrossRef]
42. Wan, X.; Zhu, J.; Lai, Y.; Lu, J.; Yan, Z. Premelting Theory-Based Mechanism for Water Freezing in Saline Soil. *Water Resour. Res.* **2024**, *60*, e2024WR038013. [CrossRef]

Disclaimer/Publisher's Note: The statements, opinions and data contained in all publications are solely those of the individual author(s) and contributor(s) and not of MDPI and/or the editor(s). MDPI and/or the editor(s) disclaim responsibility for any injury to people or property resulting from any ideas, methods, instructions or products referred to in the content.